Chapter 9

Single-Switch Differential Power Processing PWM Converter to Enhance Energy Yield of Photovoltaic Panels under Partial Shading

Masatoshi Uno, Toru Nakane and Toshiki Shinohara

Additional information is available at the end of the chapter

http://dx.doi.org/10.5772/intechopen.74307

Abstract

The partial shading on a photovoltaic (PV) panel consisting of multiple substrings poses serious issues of decreased energy yield and occurrence of multiple maximum power points (MPPs). Although various kinds of differential power processing (DPP) converters have been proposed to prevent the partial shading issues, multiple switches and/or magnetic components in proportion to the number of substrings are necessary, hence increasing the circuit complexity and volume. This chapter proposes a novel single-switch DPP PWM converter to achieve simplified circuit. The proposed DPP converter is essentially the combination of a forward/flyback resonant inverter (FFRI) and voltage multiplier (VM). The fundamental operation analysis is performed, and the current sensorless control strategy suitable for the proposed DPP converter is also discussed. A 30-W prototype of the proposed DPP converter was built, and various kinds of experimental verification tests were performed emulating partial shading conditions. With the proposed DPP converter, local MPPs of a partially shaded PV panel were successfully eliminated, and energy yield was significantly enhanced, demonstrating the efficacy and performance of the proposed DPP converter.

Keywords: differential power processing converter, forward-flyback inverter, partial shading, voltage equalization, voltage multiplier

1. Introduction

Efficient power conversion and high energy utilization are of great importance in photovoltaic (PV) power systems. Efficient power converters and inverters with maximum power point tracking (MPPT) capability have been commercialized to extract as much energy from PV

panels as possible. However, even with such efficient converters, energy yield from PV panels are known to be significantly reduced due to partial shading. A standard PV panel comprising three substrings and its characteristics under a partially shaded condition are shown in **Figure 1**. A shaded substring, PV_3, is less capable of generating current is bypassed by a parallel-connected bypass diode, and therefore, it no longer contributes to power generation, though it can potentially generate power to some extent. In addition, a partially shaded panel exhibits multiple power point maxima including global and local MPPs, which likely confuse ordinally MPPT tracking algorithms.

Partial shading issues originate from characteristic mismatch among series-connected substrings. With differential power processing (DPP) converters, power differences among substrings are transferred so that all substring characteristics are virtually unified, thus precluding the partial shading issues. Various kinds of DPP architectures have been proposed. The most straightforward architecture is the adjacent substring-to-substring equalization system, shown in **Figure 2(a)**, in which adjacent substrings exchange power difference through a DPP converter, depending on shading conditions. Bidirectional converters, such as PWM

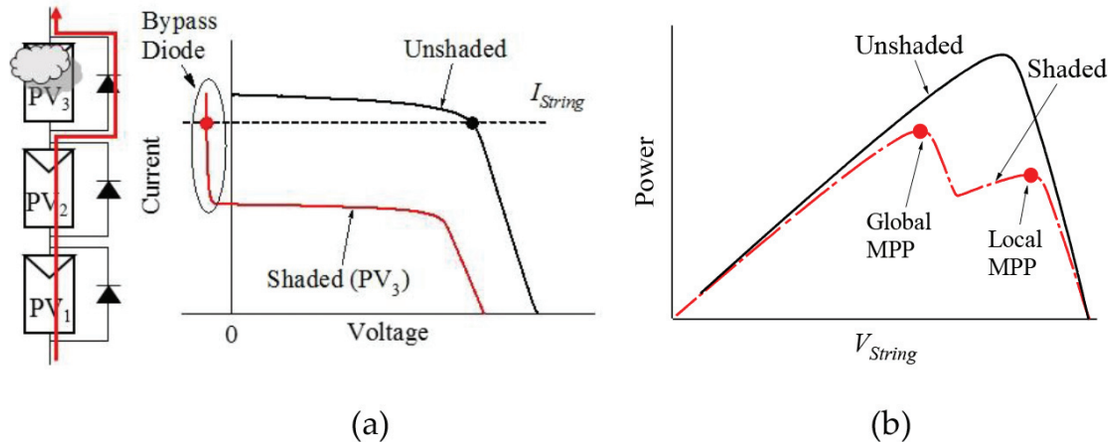

Figure 1. Characteristics of (a) substrings and (b) string under partial shading.

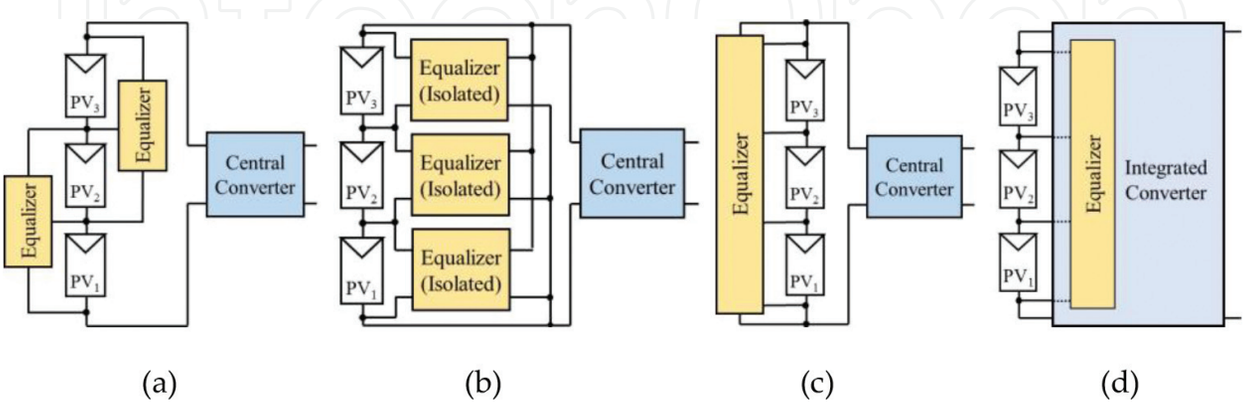

Figure 2. DPP architectures based on (a) adjacent substring-to-substring equalization, (b) substring-to-bus equalization, (c) string-to-substring equalization, and (d) integrated converter.

http://dx.doi.org/10.5772/intechopen.74307

converters [1–3] and switched capacitor converters [4, 5], are used as DPP converters in the adjacent equalization architecture. With the substring-to-bus equalization architecture shown in **Figure 2(b)**, respective bidirectional isolated flyback converter-based DPP converters transfer power between the bus and each substring [6–8]. The architectures in **Figure 2(a)** and **(b)** require multiple DPP converters in proportion to the number of substrings, likely increasing the system complexity and cost. The string-to-substring equalization architecture, on the other hand, can reduce the DPP converter count, as shown in **Figure 2(c)**. Single-input multi-output converters, such as a multi-winding flyback converter [9], multi-stacked buck-boost converters [10, 11], and LLC resonant voltage multiplier [12], can be employed as a DPP converter in this architecture. Integrated converters having a DPP converter function have also been proposed [13, 14]. The simplified system and reduced cost of the integrated converters are appealing features, but the performance as a DPP converter cannot be optimized because two converters are combined into a single unit to form the integrated converter.

From the perspective of the performance and cost, string-to-substring DPP converters are considered the most viable solution to the partial shading issues. Representative circuit topologies of the string-to-substring DPP converters are shown in **Figure 3**. Although the multi-winding flyback converter [9] (**Figure 3(a)**) is very simple as it needs only one switch, the design difficulty of the multi-winding transformer is a top concern. The multi-stacked buck-boost converter-based DPP converter is also a single-switch circuit [10, 11], but it may be bulky as multiple inductors are necessary. From the viewpoint of magnetic components, the DPP converter based on the LLC resonant voltage multiplier (VM) [12] (**Figure 3(c)**) would be the best solution, but the switch count is doubled compared to that of other string-to-substring DPP converters.

A string-to-substring single-switch DPP PWM converter based on the forward-flyback resonant inverter (FFRI) and VM is proposed in this chapter. In addition to the single-switch topology, the magnetic component count is also one, realizing the simple, easy-to-design, and miniaturized circuit. The circuit derivation and description of the proposed single-switch DPP converter are presented in Section 2, followed by the detailed operation analysis in Section 3. The current sensorless control strategy suitable for the proposed single-switch DPP converter

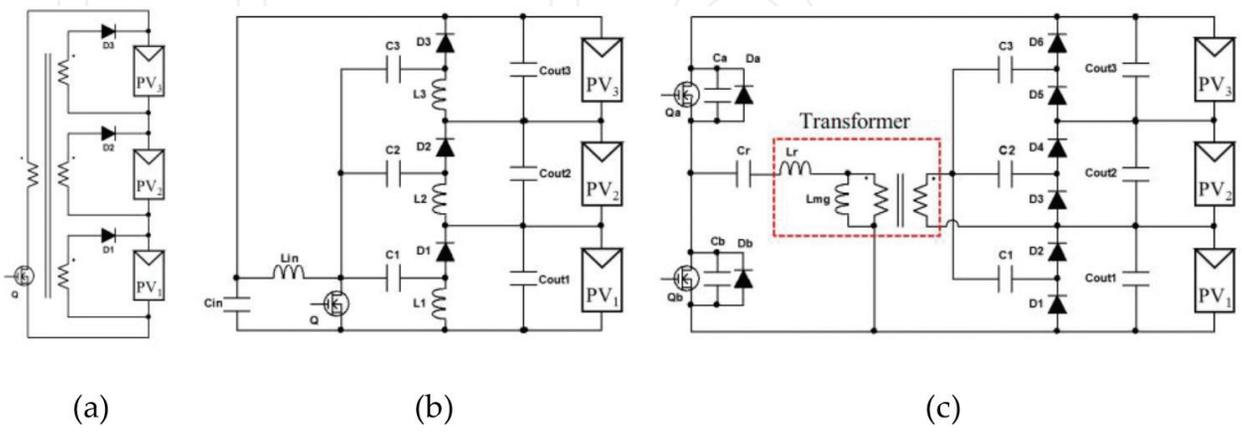

Figure 3. String-to-substring equalizers based on (a) multi-winding flyback converter, (b) multi-stacked buck-boost converters, and (c) LLC resonant voltage multiplier.

will be discussed in Section 4. The experimental results of the laboratory and field testing for a standard 72-cell PV panel consisting of three substrings will be presented in Section 5.

2. Proposed single-switch DPP converter

2.1. Key elements for proposed DPP converter

The proposed string-to-substring DPP converter is essentially the combination of the FFRI and VM, shown in **Figure 4(a)** and **(b)**, respectively. As the switch Q is turned on, the FFRI operates in the forward mode, in which the leakage inductance of the transformer, L_{kg}, resonates with the resonant capacitor C_r placed on the secondary side. At the same time, the magnetizing inductance L_{mg} stores energy. As Q is turned off, the FFRI operates in the flyback mode, and the stored energy in L_{mg} is released to the secondary side. The energy stored in L_{kg} is absorbed in a snubber circuit in order to prevent a voltage spike applied to Q. In summary, AC voltage/current is generated across the secondary winding. The detailed operation analysis will be discussed in Section 3.

The VM basically comprises multiple voltage doublers stacked in series—three voltage doublers, each consisting of a coupling capacitor, diode pair, and a smoothing capacitor, are stacked in **Figure 4(b)**. The VM is driven by AC current/voltage produced by the FFRI. The upper and lower diodes (i.e., the even- and odd-numbered diodes) alternately conduct as AC current/voltage is applied. Voltages of smoothing capacitors C_{out1}–C_{out3} are automatically unified without feedback control, and therefore, voltages of PV substrings that are connected in parallel with respective smoothing capacitors are automatically equalized. Detailed voltage equalization mechanisms can be found elsewhere [12, 14].

2.2. Circuit description of single-switch DPP converter and its features

The proposed single-switch DPP converter for three substrings is shown in **Figure 5**. The output of the FFRI is connected to the input of the VM, and therefore, the VM is driven by AC voltage/current produced by the FFRI [15]. A bias resistor R_{bias} is added to stabilize voltages of the resonant capacitor C_r and coupling capacitors C_1–C_3; C_r and coupling capacitors C_1–C_3 are connected in series, and therefore, their voltages become unstable if without a bias resistor. Although a lossless LCD snubber is employed in **Figure 5**, any snubber circuits, including traditional lossy RCD snubbers, can be used to protect the switch Q. The input of the FFRI is tied to the string, whereas the outputs (i.e., C_{out1}–C_{out3}) of the VM are connected in parallel with respective substrings. Therefore, a fraction of the string power is redistributed to shaded substrings through the proposed DPP converter so that all the substring characteristics are virtually unified even under partial shading conditions.

In addition to the single-switch topology, the magnetic component count is also only one, realizing not only simplified circuit but also miniaturized circuit design. Although the circuit shown in **Figure 5** is for three substrings, the number of substrings can be arbitrarily extended by adding diodes and capacitors in the VM, allowing a flexible design.

http://dx.doi.org/10.5772/intechopen.74307

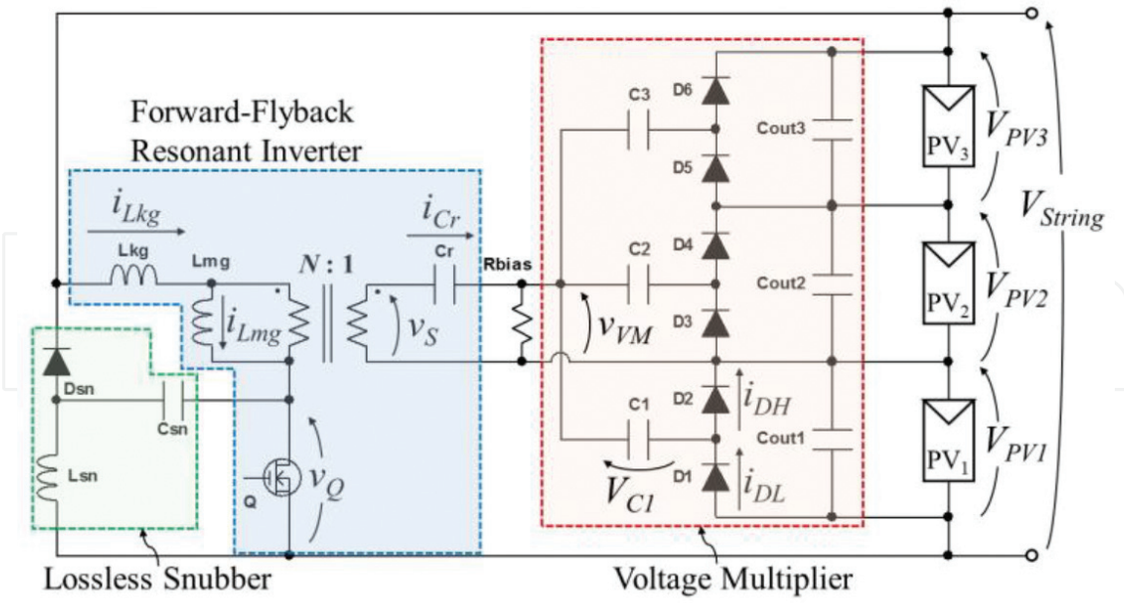

Figure 4. Proposed single-switch DPP PWM converter based on FFRI and VM.

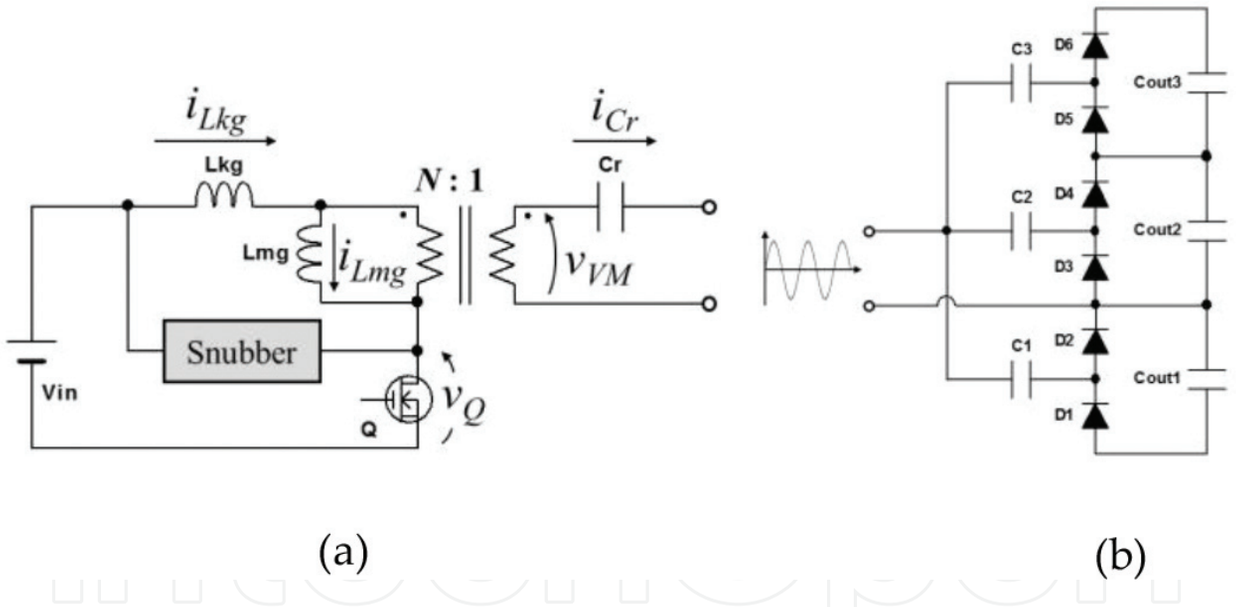

Figure 5. Key elements for proposed single-switch DPP PWM converter: (a) forward-flyback resonant inverter (FFRI) and (b) voltage multiplier (VM).

3. Operation analysis

3.1. Automatic voltage equalization mechanism

As mentioned in Section 2.2, the voltages of substrings are automatically nearly unified with the VM in the proposed DPP converter. The VM is driven by AC voltage/current generated by the FFRI, as illustrated in **Figure 4(b)**. Since capacitors C_1–C_3 are connected to the AC terminal, these

capacitors can be regarded as AC-coupling capacitors that allow AC components only to flow through them. Hence, substrings as well as parallel-connected voltage doublers, each comprising diode pairs and a coupling capacitor, can be equivalently separated and grounded, as shown in **Figure 6**. All the substrings with respective voltage doublers in this equivalent circuit are connected in parallel, and therefore, AC current preferentially flows through a voltage doubler that is connected to a shaded substring whose voltage tends to be lower than the others.

3.2. Operation principle

This section discusses the operation analysis in the case that PV_1 is partially shaded. The proposed DPP converter operates either in continuous conduction mode (CCM) or discontinuous conduction mode (DCM). The DCM operation, which contains more operation modes, is discussed in this section. Key operation waveforms and current flow directions are shown in **Figures 7** and **8**, respectively. The lossless snubber is depicted as a voltage source V_{sn} with a diode D_{sn}, in **Figure 8**, for the sake of clarity.

The average voltage of C_r is zero thanks to R_{bias} and the transformer secondary winding whose average voltage must be zero under steady-state conditions. Hence, the input voltage of the VM, v_{VM}, is nearly identical to the voltage of secondary winding, v_S.

Mode 1 (T_0–T_1) (**Figure 8(a)**): The switch Q is turned on, and the DPP converter operates in the forward mode. The current of L_{mg}, i_{Lmg}, starts linearly increasing from zero, as

$$i_{Lmg} = \frac{V_{string}}{L_{mg} + L_{kg}}(t - T_0) \tag{1}$$

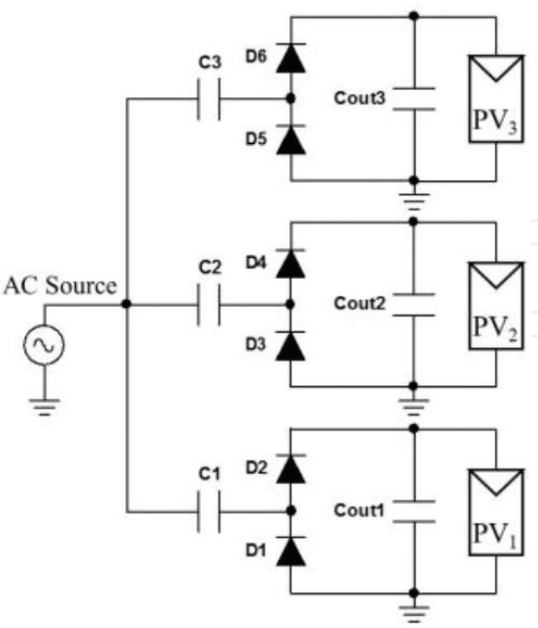

Figure 6. Equivalent circuit of voltage multiplier.

http://dx.doi.org/10.5772/intechopen.74307

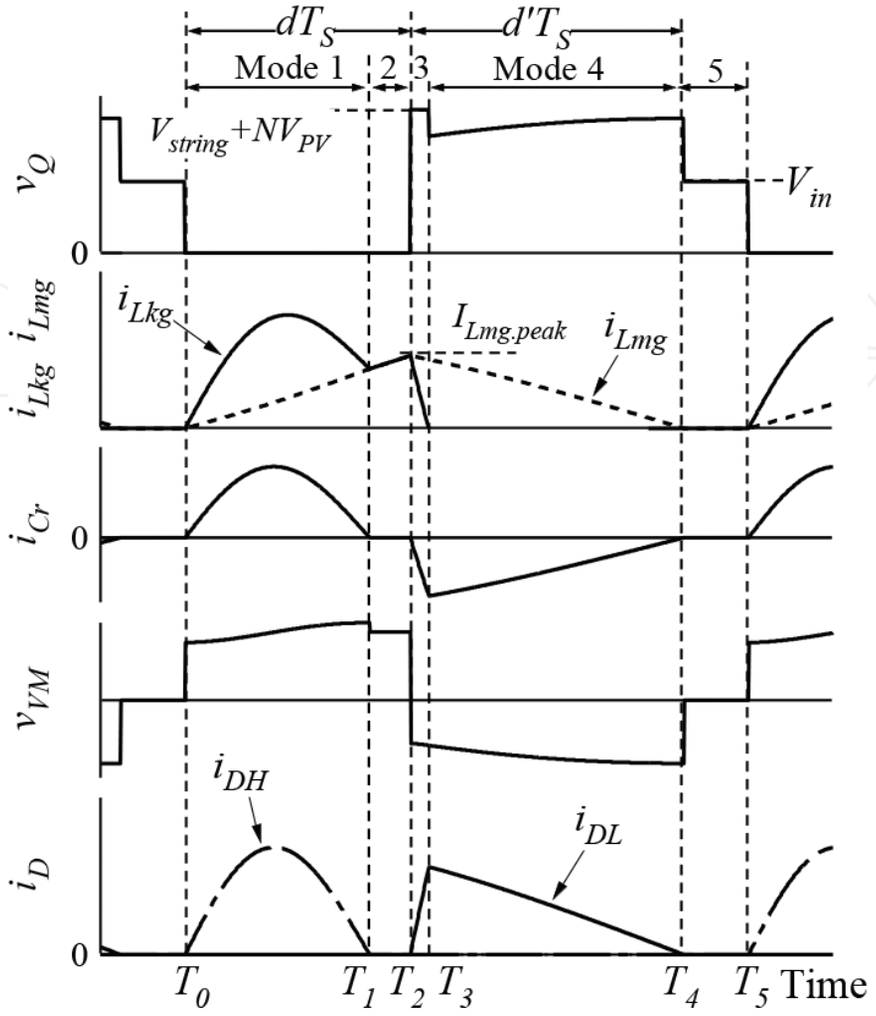

Figure 7. Key operation waveforms when PV_1 is partially shaded.

Meanwhile, L_{kg} resonates with C_r on the secondary winding, and sinusoidal current i_{Cr} flows;

$$i_{Cr} = \frac{\frac{V_{string}}{N} - V_{VM.O}}{|Z_r|} \sin \omega_r (t - T_0) \tag{2}$$

where Z_r and ω_r are the characteristic impedance of the resonant tank and resonant angular frequency given by

$$Z_r = N\sqrt{\frac{L_{kg}}{C_r}}, \omega_r = 2\pi f_r = \frac{N}{\sqrt{L_{kg}C_r}} \tag{3}$$

The current of L_{kg}, i_{Lkg}, is equal to the sum of i_{Lmg} and i_{Cr} reflected on the primary side. In the VM, the upper diode corresponding to PV_1, D_2, conducts whereas other diodes are off. Since the voltage of C_r can be approximated to be zero, v_{VM} during the even-numbered diodes are on, $V_{VM.E}$, is given by

$$V_{VM.E} = V_{C1} + V_f = \frac{L_{mg} V_{string}}{N(L_{kg} + L_{mg})} \tag{4}$$

As i_{Cr} reaches zero, this mode ends, and the operation moves to the next mode.

Mode 2 (T_1–T_2) (**Figure 8(b)**): Q is still on, but all resonant currents become zero. Since i_{Cr} is zero, i_{Lkg} is identical to i_{Lmg}. No current flows in the VM, except for the current from the smoothing capacitor C_{out1} to PV_1. In order for Mode 2 to exist, Mode 1 must be longer than half the resonant period. Hence, the following equation needs to be satisfied;

$$d \geq \frac{f_S}{2f_r} \tag{5}$$

where d is the duty cycle of Q. The peak value of i_{Lmg} at the end of this mode, $I_{Lmg.peak}$ is

$$I_{Lmg.peak} = \frac{V_{string} d T_S}{L_{mg} + L_{kg}} \tag{6}$$

Mode 3 (T_2–T_3) (**Figure 8(c)**): Q is turned off, and the DPP converter starts operating in the flyback mode. The energy stored in L_{kg} in Modes 1 and 2 is absorbed by the snubber. Meanwhile,

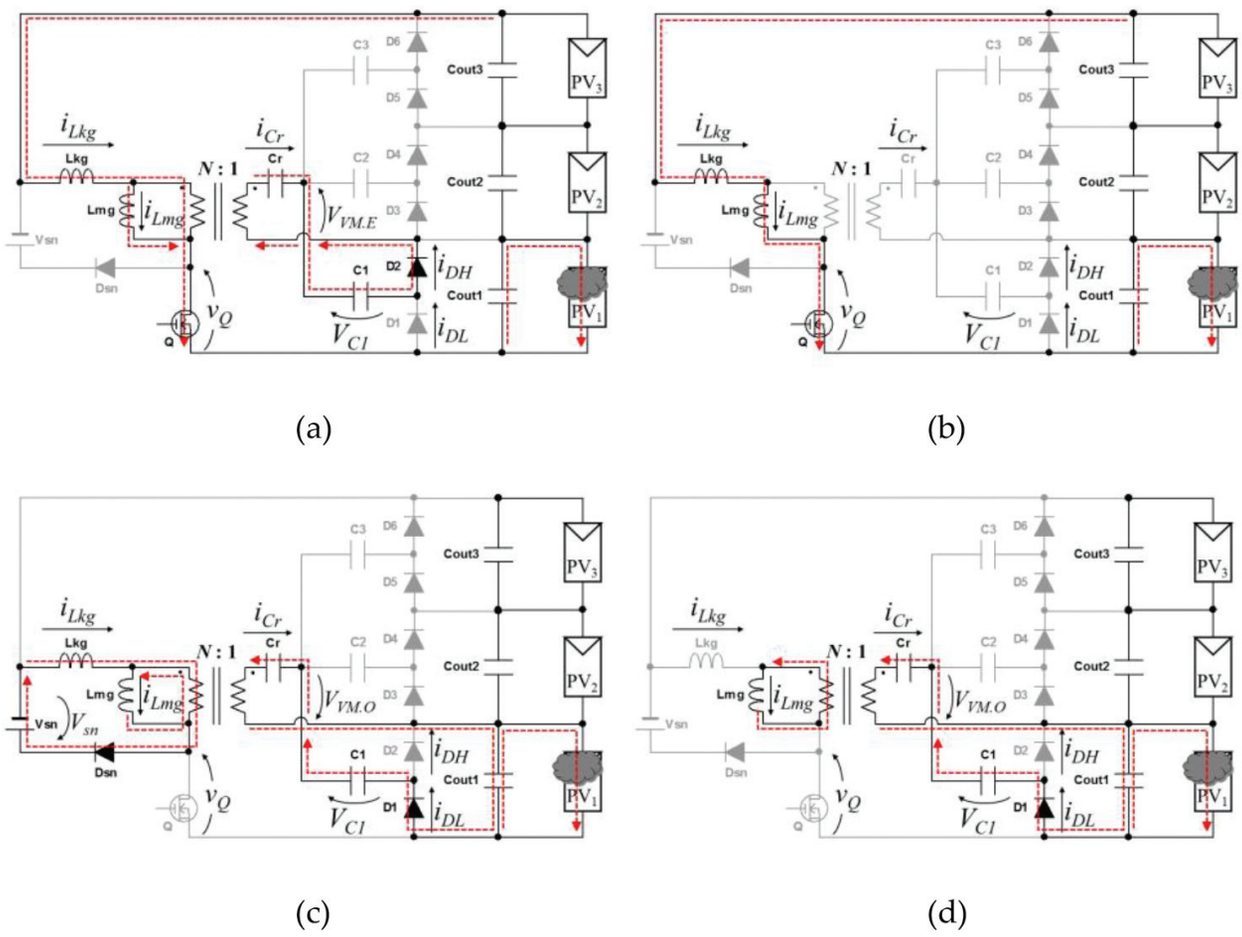

Figure 8. Current flow directions in (a) mode 1, (b) mode 2, (c) mode 3, and (d) mode 4.

i_{Lmg} begins to decrease as L_{mg} starts releasing its energy stored in the first two modes. i_{Lmg} is transferred to the secondary side, and the lower diode corresponding to PV_1, D_1, conducts. This mode ends as i_{Lkg} becomes zero—the length of this mode is practically very short compared to other modes.

Mode 4 (T_3–T_4) (**Figure 8(d)**): i_{Lmg} keeps decreasing, and its energy is released to the secondary side. i_{Lmg} in this mode is expressed as

$$i_{Lmg} = I_{Lmg.peak} - \frac{NV_{VM.E}}{L_{mg}}(t - T_3) \tag{7}$$

v_{VM} during odd-numbered diodes are on, $V_{VM.O}$, is expressed using (4) as

$$V_{VM.O} = V_{PV1} + V_f - V_{C1} = V_{PV1} + 2V_f - \frac{L_{mg}V_{stringmg}}{N(L_{kg} + L_{mg})} \tag{8}$$

The duty cycle of Mode 4, $d' = (T_3–T_4)/T_S$, is

$$d' = \frac{dV_{string}}{N(V_{PV1} + 2V_f)\frac{L_{mg}+L_{kg}}{L_{mg}} - V_{string}} \tag{9}$$

If the operation meets $d' < (1 - d)$, the DPP converter operates in DCM. The critical duty cycle for DCM operation, $d_{critical}$, is given by

$$d_{critical} < 1 - \frac{V_{string}L_{mg}}{N(L_{mg} + L_{kg})(V_{PV1} + 2V_f)} \tag{10}$$

Mode 5 (T_4–T_5) (not shown): This mode is unique to the DCM operation. No currents flow in the DPP converter, except for C_{out1} providing a current to the shaded substring PV_1.

In summary, the upper and lower diodes that are connected in parallel with the shaded substring alternately conduct. The shaded substring PV_1 receives the current from the DPP converter, whereas no current flows toward unshaded substrings.

Since the average voltage of C_r is nearly zero, v_{VM} can be assumed equal to v_S. Based on volt-second balance on the transformer secondary winding with Eqs. (4) and (8), the voltage conversion ratio of the proposed DPP converter in DCM can be yielded as

$$V_{PV1} = \frac{L_{mg}V_{string}(d + d')}{Nd'(L_{kg} + L_{mg})} - 2V_f \tag{11}$$

The voltage conversion ratio in CCM can be obtained by applying $d' = 1 – d$ into (11), as

$$V_{PV1} = \frac{L_{mg}V_{string}}{N(1 - d)(L_{kg} + L_{mg})} - 2V_f \tag{12}$$

Eqs. (11) and (12) suggest that the voltage conversion ratio is PWM-controllable, and d should be properly adjusted depending on the degree of shading. The control strategy suitable for the proposed DPP PWM converter is discussed in the next section.

4. Control strategy

There is only one single switch in the proposed DPP converter, whereas it has three outputs for PV_1–PV_3. Hence, the DPP converter needs to be properly controlled so that shaded substrings only receive a current from the DPP converter while no currents flow toward unshaded ones. To this end, the current sensorless ΔV-controlled equalization strategy [11] is employed.

The mechanism of the ΔV-controlled equalization is illustrated in **Figure 9(a)**. The proposed single-switch DPP converter can be equivalently depicted as a single-input multi-output converter with V_e and blocking diodes. Based on the ΔV-controlled equalization, the DPP converter is operated so that the voltage difference among substrings $\Delta V = V_H - V_L$ (where V_H and V_L are the highest and lowest substring voltages, respectively) is controlled to be a non-zero positive value. In this scenario, the DPP converter supplies the equalization current only for the shaded substring PV_1 whose voltage is equal to the output voltage of the DPP converter V_e. Meanwhile, unshaded substrings' voltages are higher than V_e, and therefore, currents do not flow toward them.

The control block diagram of the ΔV-controlled equalization is illustrated in **Figure 9(b)**. All the substring voltages are individually measured to calculate ΔV. The reference of ΔV, ΔV_{ref}, is set to be slightly greater than zero to be unaffected by noise.

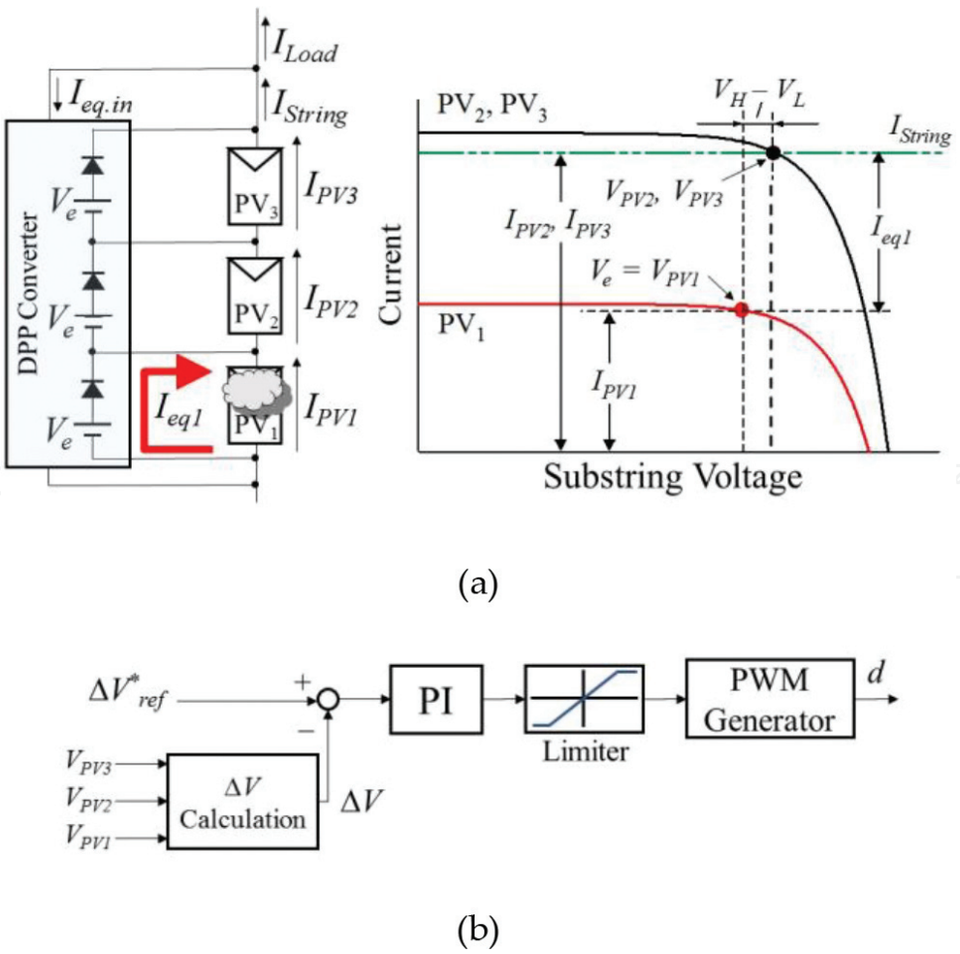

Figure 9. (a) Mechanism and (b) block diagram of ΔV-controlled equalization.

http://dx.doi.org/10.5772/intechopen.74307

5. Experimental results

5.1. Prototype

A 30-W prototype of the proposed single-switch DPP converter for standard 72-cell PV panels comprising three substrings was built, as shown in **Figure 10**. **Table 1** enlists the circuit elements used for the prototype. The prototype was operated at a switching frequency of 100 kHz, and a TMS320F28335 control card (Texas Instruments) was used to implement the ΔV-controlled equalization.

5.2. Fundamental performance

Key operation waveforms and power conversion efficiency were measured using the experimental setup shown in **Figure 11**. All substrings were removed, and the DPP converter was

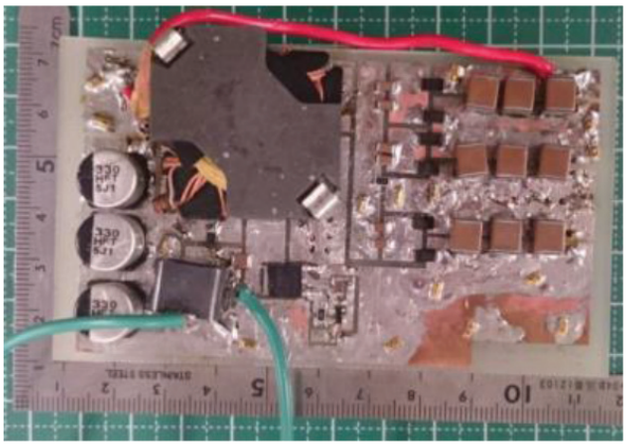

Figure 10. Photograph of the 30-W prototype.

Element	Value
Q	F390N15A, R_{on} = 33.5 mΩ
C_1–C_3	Ceramic Capacitor, 94 μF
C_{out1}–C_{out3}	Ceramic Capacitor, 300 μF
D_1–D_6	Schottkey Diode, V_f = 0.3 V
C_r	Ceramic Capacitor, 20 μF
Transformer	N_1:N_2 = 10:2, L_{kg} = 2 μH, L_{mg} = 450 μH
Snubber	C_{sn} = 2.2 μF, L_{sn} = 1 mH

Table 1. Circuit element list.

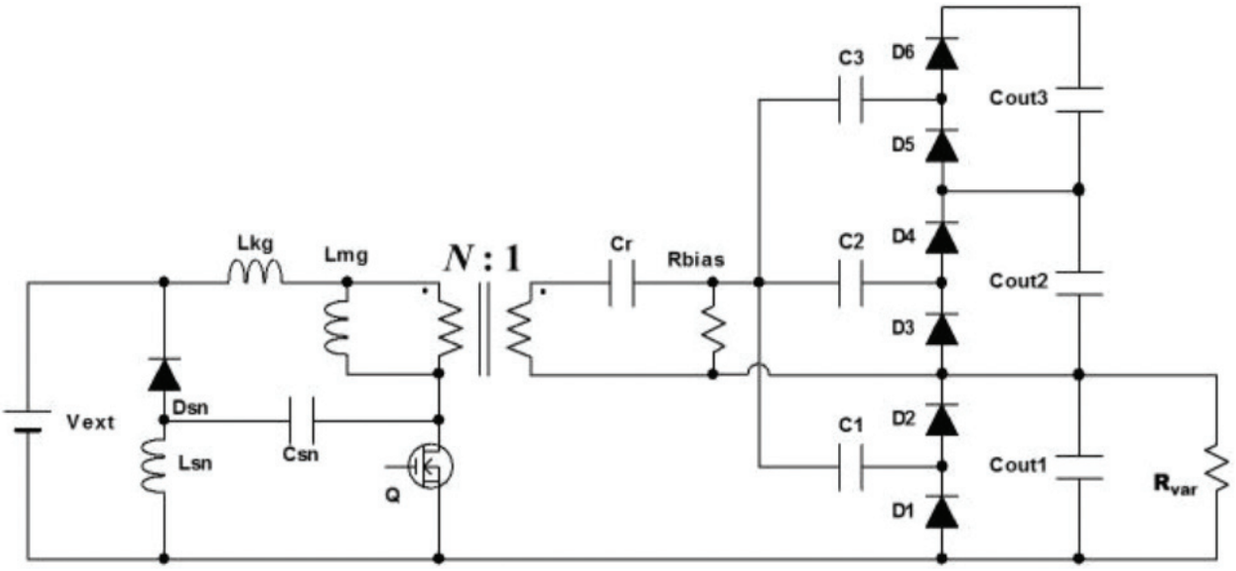

Figure 11. Experimental setup for waveform and efficiency measurement.

powered by an external power supply V_{ext}. A variable resistor R_{var} was connected to C_{out1} in order to emulate current flow directions under the PV_1-shaded condition shown in **Figure 8**.

The measured key operation waveforms in DCM are shown in **Figure 12**. Although oscillations due to the resonance between the output capacitance of the MOSFET and L_{mg} were observed in v_Q and v_{VM}, the measured waveforms matched well with the theoretical ones shown in **Figure 7**. The measured power conversion efficiency is shown in **Figure 13**. In the

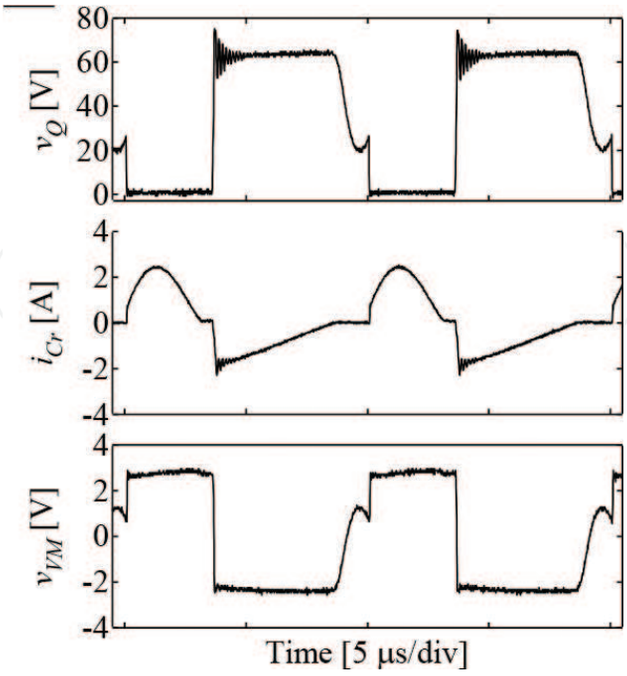

Figure 12. Measured key operation waveforms when PV_1 is partially shaded.

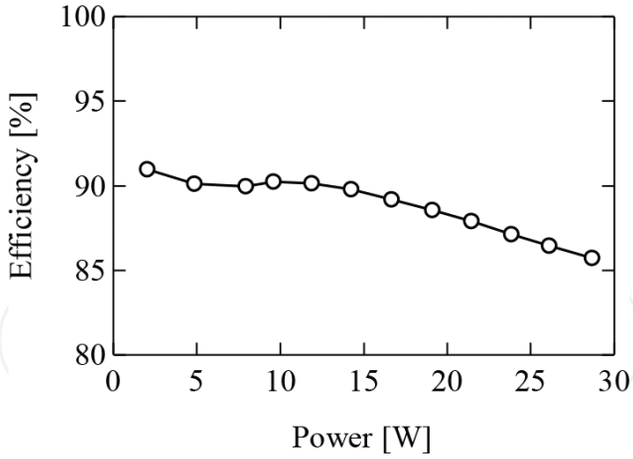

Figure 13. Measured power conversion efficiency.

light load region, the DPP converter operated in DCM and its efficiency was around 90%. The heavy load region corresponded to CCM, in which the efficiency gradually declined due to the increased Joule loss.

5.3. Laboratory testing

Solar array simulators (E4361A, Keysight Technologies) were used to emulate shaded and unshaded PV substring characteristics, as shown in **Figure 14(a)**. The short circuit current of the shaded substring PV_1 was set to be half that of unshaded substrings. String characteristics as a whole were manually swept using an electronic load operating in the resistance mode. The

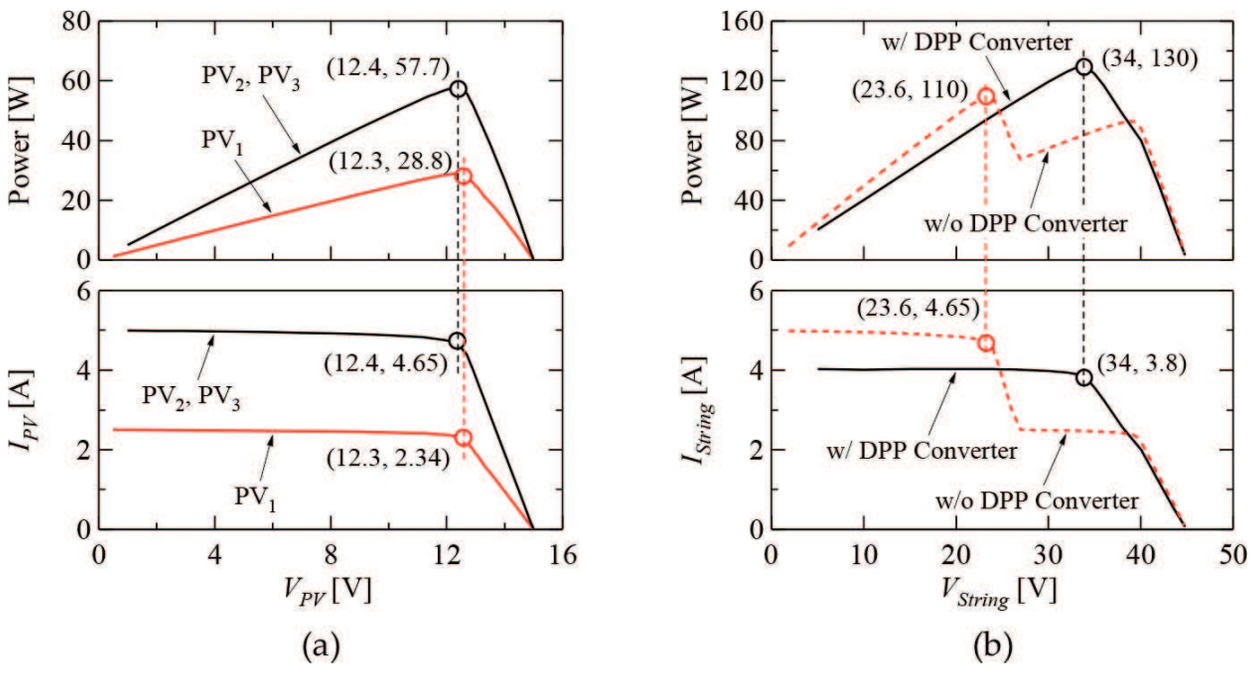

Figure 14. (a) Individual PV substring characteristics and (b) string characteristics with and without DPP converter.

ΔV-controlled equalization with ΔV_{ref} = 1.0 V was implemented. As a reference, the string characteristic without the proposed DPP converter was also measured.

Measured string characteristics with and without the DPP converter are shown and compared in **Figure 14(b)**. Without the DPP converter, two MPPs were observed, and the maximum power was merely 110 W at V_{string} = 23.6 V. With the proposed DPP converter, on the other hand, the local MPP disappeared, and maximum power increased to as high as 130 W at V_{string} = 34.0 V, corresponding to 18.2% improvement. Thus, the experimental results demonstrated the proposed DPP converter drastically increases the power yield from a partially shaded string.

The prototype of the proposed DPP converter was operated in conjunction with a commercial MPPT converter (SS-MPPT-15 L, Morningstar) to demonstrate its compatibility. The measured V_{string} and extracted power are shown in **Figure 15**. The MPPT converter periodically swept the string characteristic in search for the global MPP location and subsequently kept extracting the maximum power of approximately 130 W.

5.4. Field testing

The field test using a real PV panel was also performed emulating a partial shading condition, as shown in **Figure 16**. A standard 72-cell monocrystalline PV panel was used for the experiment, and one of the substrings was covered with a postcard to emulate a partial shading condition. The irradiance in the field test was measured using a pyranometer. The measured string characteristics with and without the proposed DPP converter prototype are shown in **Figure 17**. Without the DPP converter, two power maxima were observed, and the extractable maximum power was approximately 39 W at the irradiance level of 372 W/m^2. With the DPP converter, the maximum power increased to as high as 46.1 W, in spite of the lower irradiance level of 356 W/m^2.

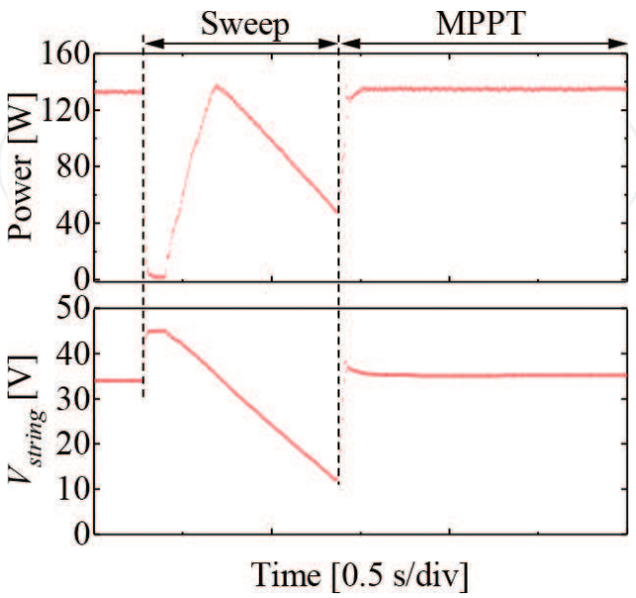

Figure 15. Measured power conversion efficiency.

http://dx.doi.org/10.5772/intechopen.74307

Figure 16. Field test setup.

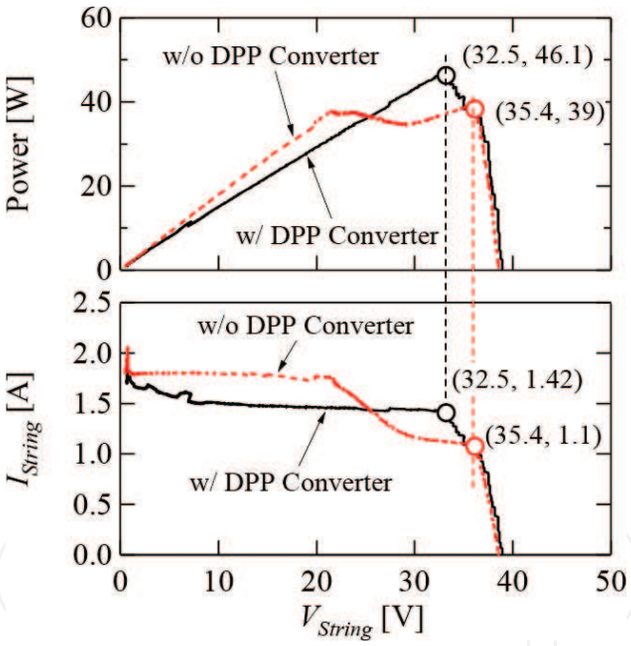

Figure 17. String characteristics with and without DPP converter in the field test.

6. Conclusions

The single-switch DPP PWM converter to preclude the partial shading issues has been proposed in this chapter. The proposed DPP converter can be derived by integrating the FFRI and VM into a single unit. The switch count of the proposed DPP converter is only one, thus achieving the simplified circuit. The operation analysis was performed, and the voltage conversion ratios in DCM and CCM were mathematically yielded.

The 30-W prototype of the proposed DPP converter was built, and its fundamental operation performance was measured. Experimental equalization tests emulating partial shading conditions were performed using solar array simulators or a real PV panel. With the prototype of the proposed DPP converter, local MPPs disappeared, and extractable maximum powers significantly increased, demonstrating the efficacy and performance of the proposed DPP converter.

Author details

Masatoshi Uno*, Toru Nakane and Toshiki Shinohara

*Address all correspondence to: masatoshi.uno.ee@vc.ibaraki.ac.jp

Ibaraki University, Hitachi, Japan

References

[1] Bergveld HJ, Büthker D, Castello C, Doorn T, Jong AD, Otten RV, Waal KD. Module-level dc/dc conversion for photovoltaic systems: The delta-conversion concept. IEEE Transactions on Power Electronics. 2013;**28**:2005-2013. DOI: 10.1109/TPEL.2012.2195331

[2] Shenoy PS, Kim KA, Johnson BB, Krein PT. Differential power processing for increased energy production and reliability of photovoltaic systems. IEEE Transactions on Power Electronics. 2013;**28**:2968-2979. DOI: 10.1109/TPEL.2012.2211082

[3] Shimizu T, Hashimoto O, Kimura G. A novel high-performance utility-interactive photovoltaic inverter system. IEEE Transactions on Power Electronics. 2003;**18**:704-711. DOI: 10.1109/TPEL.2003.809375

[4] Stauth JT, Seeman MD, Kesarwani K. Resonant switched capacitor converters for submodule distributed photovoltaic power management. IEEE Transactions on Power Electronics. 2013;**28**:1189-1198. DOI: 10.1109/TPEL.2012.2206056

[5] Chang AH, Avestruz AT, Leeb SB. Capacitor-less photovoltaic cell-level power balancing using diffusion charge redistribution. IEEE Transactions on Power Electronics. 2015;**30**: 537-546. DOI: 10.1109/TPEL.2014.2340403

[6] Olalla C, Clement D, Rodríguez M, Makisimović D. Architectures and control of submodule integrated dc-dc converters for photovoltaic applications. IEEE Transactions on Power Electronics. 2013;**28**:2980-2997. DOI: 10.1109/TPEL.2012.2219073

[7] Jeon YT, Lee H, Kim KA, Park JH. Least power point tracking method for photovoltaic differential power processing systems. IEEE Transactions on Power Electronics. 2017;**32**: 1941-1951. DOI: 10.1109/TPEL.2016.2556746

[8] Chua G, Wena H, Jiangb L, Hub Y, Lia X. Bidirectional flyback based isolated-port submodule differential power processing optimizer for photovoltaic applications. Solar Energy. 2017;**158**:929-940. DOI: 10.1016/j.solener.2017.10.053

[9] Du J, Xu R,Chen X, Li Y ,Wu J. A novel solar panel optimizer with self-compensation for partial shadow condition. In: Proceedings of the IEEE Applied Power Electronics Conference and Exposition. (APEC); 27 May 2013; Long Beach. California: IEEE; 2013. p. 92-96

[10] Uno M, Kukita A. Single-switch voltage equalizer using multi-stacked buck–boost converters for partially-shaded photovoltaic modules. IEEE Transactions on Power Electronics. 2015;**30**:3091-3105. DOI: 10.1109/TPEL.2014.2331456

[11] Uno M, Kukita A. Current sensorless equalization strategy for a single-switch voltage equalizer using multistacked buck–boost converters for photovoltaic modules under partial shading. IEEE Transactions on Industry Applications. 2017;**53**:420-429. DOI: 10.1109/TIA.2016.2615022

[12] Uno M, Kukita A. Two-switch voltage equalizer using an LLC resonant inverter and voltage multiplier for partially shaded series connected photovoltaics modules. IEEE Transactions on Industry Applications. 2015;**51**:1587-1601. DOI: 10.1109/TIA.2014.2336980

[13] Uno M, Kukita A. PWM converter integrating switched capacitor converter and series-resonant voltage multiplier as equalizers for photovoltaic modules and series-connected energy storage cells for exploration rovers. IEEE Transactions on Power Electronics. 2017; **32**:8500-8513. DOI: 10.1109/TPEL.2016.2645705

[14] Uno M, Kukita A. Single-switch single-magnetic PWM converter integrating voltage equalizer for partially-shaded photovoltaic modules in standalone applications. IEEE Transactions on Power Electronics. 2018;**33**:1259-1270. DOI: 10.1109/TIA.2014.2336980

[15] Uno M, Kukita A. Single-switch single transformer cell voltage equalizer based on forward–flyback resonant inverter and voltage multiplier for series-connected energy storage cells. IEEE Transactions on Vehicular Technology. 2014;**63**:4232-4246. DOI: 10.1109/TVT.2014.2312381

IntechOpen